NASA Contractor Report 3413

An Implicit Method for the Calculation of Inlet Flow Fields

Sedat Biringen and O. J. McMillan

CONTRACT NAS1-15951
JUNE 1981

NASA

NASA Contractor Report 3413

An Implicit Method for the Calculation of Inlet Flow Fields

Sedat Biringen and O. J. McMillan
Nielsen Engineering & Research, Inc.
Mountain View, California

Prepared for
Langley Research Center
under Contract NAS1-15951

NASA
National Aeronautics
and Space Administration

**Scientific and Technical
Information Branch**

1981

TABLE OF CONTENTS

SUMMARY

Inlet flow fields are calculated by an implicit, time-marching procedure to solve the thin-layer Navier-Stokes equations formulated in body-fitted coordinates. Because the method can be used for a flow field with both subsonic and supersonic regions, it is applicable to subcritical as well as supercritical inlet operation.

Results are presented and discussed for an inlet of current design practice. Results include inviscid calculations performed for supercritical inlet operation with uniform and nonuniform inflow boundary conditions as well as for subcritical inlet operation with uniform inflow boundary conditions. Results for viscous calculations performed for supercritical inlet operation with uniform inflow boundary conditions are also discussed.

1. INTRODUCTION

Inlet flow fields for high-speed airbreathing missiles are very complex due to their mixed hyperbolic-elliptic nature, and the fact that the flow field is influenced by the missile forebody. These flow fields are, of course, also influenced by viscous effects and are highly three-dimensional, and a fully accurate prediction of such flows requires the inclusion of all these phenomena. Despite the difficulties involved, the successful performance of such calculations is of considerable importance to the efficient design of an air-breathing missile, e.g. to maximize total pressure recovery and to minimize cowl drag due to spillage at off-design conditions.

This report is a summary of our work on the computation of inlet flow fields for air-breathing missiles in a supersonic free stream wherein an attempt is made to deal with all of the complex elements of two-dimensional flow fields; this is viewed as an important evolutionary step in the direction of the solution of the fully three-dimensional problem. The effects of the forebody are included in these inlet calculations through nonuniform boundary conditions which are generated via a space-marching technique which solves the three-dimensional Euler equations around the forebody. Details of the code used to solve the forebody flow field and several test cases run using the forebody code are given in references 1 and 2. Our approach for calculating the inlet flow field is to use a recently developed implicit time-marching solution technique (refs. 3 and 4) for numerically solving the governing equations. Either the time-dependent Euler equations (inviscid) or the time-dependent Navier-Stokes equations with the thin-layer approximation (viscous effects) are solved.

The calculation of inlet flow fields by the use of finite difference techniques has been the subject of a number of

investigations. Explicit time-marching finite difference techniques have been used (e.g., refs. 5, 6 and 7) to solve the Euler equations for transonic and supersonic flows in inlets. For explicit methods, the Courant-Friedrichs-Lewy (CFL) (ref. 6) stability criterion restricts the allowable time-step and hence for finely clustered meshes (e.g. near solid boundaries where the flow field gradients are very large) convergence rates are very slow. Other available methods (for example, refs. 8 and 9) are limited to supersonic flows and thus cannot be applied to the important case of subcritical inlet operation. The present work is an attempt to overcome these restrictions by using a time-marching implicit scheme; the implicit solution technique in many cases allows step sizes much larger than those obtained from the CFL criterion for explicit methods, whereas the use of time-dependent equations permits the calculation of subsonic, as well as supersonic, internal flows without having to switch difference operators.

The objectives of this work are two-fold. The first one involves a detailed calculation of the flow field in and about a practical inlet configuration. The calculation is structured so as to focus on the external aerodynamic effects of the inlet, i.e., the captured mass flow and the external forces due to the ramp and cowl. Inlet internal performance is not emphasized in the present work, although some information in this area is available from our results. Inviscid calculations are performed and results are presented for supercritical and subcritical inlet operation with uniform and non-uniform inflow boundary conditions. Calculations are also performed including viscous effects which are simulated by the thin-layer Navier-Stokes equations. Our second objective involves a critical assessment of the present calculation procedure from a user's point of view. Consideration is given to special techniques necessary to achieve convergence, the convergence criteria used, and the convergence time necessary to obtain solutions.

All the calculations were performed for the inlet configuration shown in figure 1. This inlet has a shock-on-cowl design Mach number of 3.5, a 5° ramp and a sharp-lipped cowl with an initial external angle of 20°. Subsonic and transonic test results for this inlet configuration are presented in reference 10. A supersonic test series is planned by NASA/ Langley Research Center. For our calculations, a short constant-area channel has been added downstream of the subsonic diffuser to simplify the specification of flow conditions at the duct exit plane. This inlet is representative of current design practice and is a stringent test of the calculation procedure.

2. SOLUTION PROCEDURE

In this section, brief descriptions are given of the solution procedures employed for the calculation of inlet flow fields and of the mesh generation technique. More detail is available in references 4, 11 and 12.

2.1 Solution Procedure for Inlet Flow Fields

The solution procedure employs the Navier-Stokes equations for two-dimensional plane flows written in conservation-law form for a perfect gas without body forces. In the inviscid code, these become the Euler equations. Otherwise, the thin-layer assumptions are employed. In order to allow the use of a body-fitted coordinate system, the equations are subjected to a general independent variable transformation. In the problem under consideration, four types of boundaries are considered (fig. 2). These are solid boundaries, inflow boundaries, outer boundaries and outflow boundaries. For inviscid calculations, along the cowl and ramp surfaces the tangency condition is satisfied whereas the no-slip conditions are satisfied in the case of viscous calculations. In both cases the pressure on the body surface is found from the normal momentum equation.

Free-stream values are specified at the inflow and outer boundaries. At the outflow boundary, for supercritical inlet conditions, all the flow field variables are calculated by zeroth-order extrapolation from the interior. For subcritical operation (subsonic duct outflow), extrapolation is used outside the inlet, but at the duct outflow boundary the velocity component parallel to the outflow boundary, v, is set to zero and the pressure, p, is set equal to a constant value for compatibility with the steady-state momentum equation in the direction normal to the body surface. Then in accordance with the equations of continuity and streamwise momentum, u and ρ (streamwise velocity and density, respectively) are calculated by zeroth-order extrapolation.

The initial conditions are specified by using either free-stream conditions, or the final solution of a previously calculated flow field. For economy the inlet boundary has been placed just downstream of the ramp leading edge. On this boundary, when starting from free-stream conditions, values calculated from oblique shock theory are used at the 3-5 points on the inflow boundary that are downstream of the ramp shock.

The solution procedure employs a temporal linearization process; the linearized equations are cast into delta-form algorithm after approximate factorization. The inlet flow field is obtained as the steady-state solution of the time-marching method.

2.2 Mesh Generation

The main advantage of using the governing equations in transformed form is that a body-fitted coordinate system in the physical plane can be mapped onto a rectangular coordinate system in the computational plane. Moreover, grid points can be clustered in regions where there are large gradients of the

field variables. In this work the computer code of reference 13 for the application of the Thames, Thompson, and Mastin (ref. 14) (TTM) method to generate body-fitted coordinates for airfoils was modified for the inlet geometry.

The simplest form of the TTM method solves Laplace's equations in the physical plane, x-y, to generate curvilinear coordinates $\xi(x,y)$, $\eta(x,y)$ in the transformed plane. The solution of these equations for x and y on the rectangular ξ,η computational plane yields the mesh in the physical plane. One of the most desirable aspects of the TTM method is the ability to arbitrarily locate boundary points by specifying their locations in the x,y-plane.

An option is provided to cluster grid points near the cowl internal and external surfaces and the ramp surface for increased accuracy in regions where the flow field variables have large gradients. To this end an exponential clustering transformation (ref. 15) was employed which clusters grid points near each surface.

3. RESULTS

In this section detailed results are presented and discussed. All the calculations were performed at the design Mach number, $M_\infty = 3.5$. Section 3.1 consists of the presentation of the grids generated for the inviscid and viscous calculations. In section 3.2 results are presented for the inviscid calculations. Supercritical and subcritical inlet operation with uniform inflow boundary conditions and supercritical operation with non-uniform inflow boundary conditions are included. Section 3.3 contains the results obtained from the calculations including viscous effects for supercritical operation. Comparison of these results with experimental data awaits the completion of the previously mentioned test series to be conducted by NASA/Langley Research Center.

3.1 Grid Generation and Mesh Systems

In computational methods that make use of body-fitted coordinate systems, the calculation of the metric coefficients as well as the grid system incorporated have a very large effect on the accuracy, stability and covergence of the solution (ref. 4). Since a detailed study of these factors was well beyond the scope of the present work, we have found it necessary to follow certain general guidelines. In the calculation procedure of reference 4, the metric coefficients that appear in the transformed form of the governing equations are calculated by differencing the x-y values in the transformed plane. Minimum error is introduced for constant values of the dependent variables if identical finite-difference operators are used to evaluate the metric terms and the spatial derivatives in the transformed equations. Moreover, the dependent variables should vary smoothly and gradually with ξ and η and this in turn requires a smoothly varying grid.

The grid generated for the inviscid calculations is presented in figures 3 and 4. About 30 sec. on the CDC 7600 was required to generate this 73x26 grid system. This grid was used for calculations with uniform and non-uniform inflow conditions. The outer boundary of the grid is chosen so as to include the bow shock from the forebody in the case of calculations using non-uniform initial conditions. The grid system has 26 lines at constant η and 73 at constant ξ. Figures 3 and 4 display that the grid near the inlet surfaces meets the previously mentioned requirements fairly well, although improvements could generally be made. The grid is well clustered in the region around the cowl tip and at the ramp initial station to correctly capture the location and strength of the resulting shock system. However, the grid is coarse in the external flow field far from the cowl and the results in that area should be expected to be inaccurate. This area is not important for our

present purposes, and these inaccuracies are not expected to affect the results of interest in an important way. Grid refinement studies would be of interest, of course, but are beyond the scope of the present work.

In the case of generating a grid to be used in the calculations with the inclusion of viscous effects, the following additional points have to be considered.

1. It is usually considered necessary to have fine mesh resolution only in the y-direction (refs. 7 and 16), i.e. in the viscous-dominated portions of the flow field, $\Delta y \simeq \delta/10$ where δ is the boundary layer thickness. This, of course, requires an a priori estimate of the boundary layer thickness; we have considered turbulent flow only, for which we have used $\delta/x = 0.37(Re_x)^{-1/5}$. For the case considered here, the Reynolds number is 3.3×10^6/m.

2. For the turbulence model used (ref. 17), it is desirable that the first mesh point away from the solid boundary be placed in the laminar sublayer. Noting that the laminar sublayer thickness, y_s, is usually about $y_s \simeq 10^{-3}\delta$, for a given grid, y_s can be estimated from $y_s/x \simeq 0.37 \times 10^{-3}(Re_x)^{-1/5}$. In the present calculation we have placed the first mesh point away from the wall (y_{min}) at 5.1×10^{-5} m; for most of the flow field this satisfies the condition $y_{min} \leq y_s$. Other authors have used $y_{min} = 0.7 \times 10^{-5}$ m at $Re_x = 36 \times 10^6$/m (ref. 4) and $y_{min} = 3 \times 10^{-5}$ m for $Re_x = 10^6$/m (ref. 18).

The grid system resulting for the viscous calculations was similar to that used in the inviscid calculations except that there were 36 lines at constant η. It should be noted that in the present calculations with 10-12 points in each of the boundary layers (of the ramp and the cowl) the flow outside these regions is resolved by only 12-16 mesh

points. As stated previously, this should be expected to give erroneous results in those regions of the outer rotational flow where the flow field variables have steep gradients. This compromise has been made to conserve the available computer funds.

3.2 Inviscid Flow Calculations

In this section we present and discuss the results of our inviscid calculations. Attention is paid to calculation strategy as well as convergence criteria and convergence times. Section 3.2.1 consists of the results for an inlet with supersonic duct outflow conditions (supercritical operation) with uniform inflow boundary conditions. A subcritical inlet flow field solution (subsonic duct outflow conditions) with uniform inflow boundary conditions is presented in section 3.2.2 and section 3.2.3 consists of the results for a supercritical case with non-uniform inflow boundary conditions.

3.2.1 Supercritical solution with uniform inflow boundary conditions.- In explicit methods the step size in the marching direction is bounded by the CFL condition. In this case the step size must be chosen such that the Courant number will be always less than or equal to one. In implicit schemes linear stability theory suggests that this condition may be relaxed and Courant numbers much larger than one are sometimes possible without the solution becoming unstable. In the present supercritical case, although Courant numbers up to 50 were used, the following techniques were necessary to avoid stability problems.

1. Calculations had to be made for about 40 time steps at a Courant number of one (without the cowl present) to capture the ramp shock.

2. The cowl boundary conditions then had to be introduced into the calculation over some 50 time steps. The Courant number could then be increased up to 50.

Results from these calculations are shown in figures 5-9. In figure 5, the ramp surface pressure distributions obtained from the present calculations are compared with values obtained using two-dimensional shock theory and Prandtl-Meyer turning analysis. Good agreement is shown. In figure 6, a similar comparison is shown for the surface pressure distribution on the initial portion of the cowl inner surface. Except in the immediate vicinity of the cowl tip, i.e., at around $x = .4$ m, fair agreement is shown for the two results, although the Euler calculation results are generally lower. The discrepancy at the cowl tip is likely due to a combination of a singularity introduced by the very sharp cowl tip and the smearing caused by the shock-capturing process. Figure 7 shows the pressure contours for the entire flow field, whereas figure 8 shows the details of the pressure contours around the cowl tip. These figures display that while the initial ramp shock and the shock at the cowl tip are captured, a considerable amount of smearing has occurred. Also the effects of the coarse grid are very evident in the flow field calculated outside the ramp shock.

In figure 9 the convergence history of the calculations for this case are detailed. In estimating the progression of the solution to convergence, we have examined the time-behavior of two quantities. The first of these quantities is the residual, $\partial\hat{q}/\partial t$ where $\hat{q}$ is the solution vector in the transformed coordinate system. Since we are seeking steady state solutions, the desired solution will be obtained when $\partial q/\partial t \to 0$, indicating that the solution is not changing in time. We have also examined the time history of the captured mass flow ratio, $\dot{m}$, as another indication of convergence. The choice of $\dot{m}$ to indicate convergence of the solution is due to the fact that it is representative of the interesting integral parameters of the flow field and these integral parameters tend to converge faster than more detailed quantities. However, we found that $\dot{m}$

calculated at different cross-sectional locations within the inlet duct varies somewhat during convergence, so the value plotted in figure 9 has been averaged over a number of cross-sections within the inlet. In figure 9, the behavior of these quantities indicates that the solution has converged in about 800-1000 time-steps. As expected, the value of $\dot{m}$ is equal to one once the solution converges and in the converged solution, a section-to-section variation of only 1% exists. The calculations take about 0.75 sec. of CPU time per time step on the CDC 7600 computer at NASA/ARC. Hence the total CPU time spent on a typical supercritical flow solution is about 600-750 sec.

3.2.2 Subcritical solution with uniform inflow boundary conditions.- The converged solution described above was used to initiate a subcritical calculation. The back pressure at the duct outflow boundary was set to a value high enough to ensure subsonic outflow, namely $P_B = 0.7P_{T_\infty}$, where P_{T_∞} is the total pressure in the free stream. In order to make the normal shock (that is formed at the outflow boundary because of the boundary conditions imposed there) march upstream, the value of P_B was slowly increased to its full value over about 200 time steps. This pseudo time-dependency of the outflow boundary condition was found to be absolutely necessary to make the shock move regardless of the value of P_B. During the integration process various measures had to be taken in order to preserve numerical stability.

1. A Courant number of at least 10 could be used while there was supersonic flow throughout the duct. To keep the calculation stable when the duct flow was nearly all subsonic, however, the Courant number had to be decreased to one.

2. A special "pressure smoothing" had to be applied in the inlet almost all the way from the cowl-tip plane to the inlet exit plane for about 6500 time-steps. This smoothing consisted of averaging the pressure at adjacent points after each time

integration step; since it did not alter the structure of the main computation procedure, this additional smoothing did not affect the implicit stability properties of the integration procedure.

With these measures a solution was obtained, but it was observed that owing to the smoothing introduced to damp numerical instabilities, the solution was not physically realistic. Hence, after about 6500 time steps the pressure smoothing technique was used only in a region very close to the cowl tip, where it was still found to be required. In figures 10-12 surface pressure distributions for this case are shown for three instants in time. In figure 10, the pressure distribution on the ramp surface at 8500 steps shows a steeper gradient than the one at 7500 and the region of large pressure gradient has moved upstream with increasing steps, lending support to the idea that the solution will improve further with increasing steps. Pressure distributions on the cowl inner and outer surfaces (figs. 11 and 12) reveal a similar dependence on increasing steps. Density contours for this case are shown in figure 13 at 8500 steps, in which the sonic line is shown to be near the cowl tip plane. It should be noted that the ramp leading-edge shock is still smeared over a fairly large number of grid points and that the terminal normal shock is not yet captured. Convergence history of the solution for these calculations is shown in figure 14. Each sharp increase in the residual corresponds to a change in the calculation input, e.g. decrease of Courant number or a local application of the smoothing operator. The trends displayed by both parameters, i.e. the residual and $\dot{m}$, show that even at 8500 steps the calculation is not yet converged. Hence, it is our estimate that a much larger number of time-steps will be required to satisfy the convergence criteria that we have used herein.

3.2.3 Supercritical solution with non-uniform inflow boundary conditions.- The capability of the method to calculate a realistic situation in which the inlet is immersed in the flow field produced by a forebody was tested by using non-uniform inflow boundary conditions. To this end the computer code detailed in references 1 and 2 was used to generate a solution at $M_\infty = 3.5$ and at zero angle of attack for a forebody consisting of a 2.46 caliber von Karman ogive nose coupled to a cylindrical section (fig. 15). The ratio of body diameter to inlet capture height was taken equal to three, which is representative of a realistic configuration.

The solution at $x/D = 4.5$ was used as the inflow boundary condition for the inlet calculation. On this boundary, the Mach number varied from 3.465 near the ramp to 3.192 at the farthest point from the ramp within the forebody shock. For reasons of economy we have again located this boundary just downstream of the ramp leading edge. We have, therefore, assumed the first four points on this boundary away from the ramp surface to be downstream of an oblique shock with a constant 3.465 upstream Mach number. We do not expect this to introduce any significant error because the actual maximum Mach number variation over these four points was about 1%. For all the other points outside the ramp shock, exact values from the forebody solution were used as described in reference 11.

The method of transforming variables from one program output to the other program input is discussed in reference 11. In the subsequent supercritical inlet calculation a similar strategy was used to that of section 3.2.1, that is, calculations had to be done initially at a Courant number of one (without the cowl present) to capture the ramp shock, the cowl then had to be introduced into the calculation over some 40 time steps. Finally, as the cowl boundary conditions were slowly introduced, the Courant number was increased up to 50.

Results for these calculations are shown in figures 16-19. In figure 16 the surface pressure distributions on the ramp for this case are compared with the results from the calculations with uniform initial conditions. As expected, surface pressures from this case are significantly higher due to the presence of the forebody shock, although the general trends displayed by both calculations are similar. The same trends are observed in figure 17, which displays the surface pressure distributions on the cowl inner surface for the two supercritical flow solutions with uniform and non-uniform initial conditions. Owing to the reduced Mach number at the inlet due to the forebody shock, the non-uniform initial conditions result in significantly higher surface pressures. Pressure distributions on the cowl outer surface are shown in figure 18, which also displays higher pressures for the case of non-uniform inflow boundary conditions.

Details of the convergence history for these calculations are given in figure 19. These indicate that the solution converges at about 1500 time-steps and that the mass flow ratio is about 8% less than the mass flow ratio obtained with uniform initial conditions. Note that U_∞ is used to calculate $\dot{m}$ in all cases.

3.3 Viscous Flow Solution

In this section we discuss the results of our viscous calculations for a supercritical case. Viscous effects are represented by the two-layer eddy-viscosity turbulence model of reference 17. The details of the model and its incorporation into the governing equations via the thin-layer approximation are discussed in reference 12. For these calculations a 73x36 grid was generated as explained in section 3.1, which enabled the resolution of each of the turbulent boundary layers on the ramp and the cowl by about 10 mesh points. For most of the flow

field the first mesh point away from the wall lies in the laminar sublayer.

On the solid boundaries no-slip conditions were utilized for the velocities and the pressure is found from the normal momentum equation. Boundary conditions on the outer and outflow boundaries were imposed as for the inviscid case. On the inflow boundary, again taken just downstream of the ramp leading edge, inviscid boundary conditions were employed for simplicity; that is, no attempt was made to represent the ramp boundary layer at this station.

The calculation strategy followed was similar to that for the previous supercritical cases but differed in detail: Starting with a Courant number of one and increasing successively to 100 over some 1500 time-steps, the ramp flow field was calculated alone until the solution was changing only slowly in time. No numerical stability problems were encountered for this portion of the calculation.

Once the ramp flow field was established (with the proper ramp shock and boundary-layer type velocity profiles), the cowl was slowly introduced into the calculation over some 40 time-steps at the same time the Courant number was decreased to one. In about 300 time-steps the computation started to produce instabilities around the cowl tip and the ramp leading edge. We have been able to suppress the former by using a pressure-smoothing operator in the vicinity of the cowl tip but we have not been able to alleviate the numerical instabilities near the ramp leading edge. We attribute the occurrence of these instabilities to the following.

(a) Insufficiently smoothly-varying mesh. The stability of the computation depends on the modulus of the local eigenvalues of the iteration matrix which is a function of the coefficient matrices; the greater the modulus the smaller

the permissible time-step. Since the coefficient matrices are, in turn, functions of the metric coefficients, the value of the modulus increases in regions where the coordinate lines change abruptly, e.g., close to the ramp at the inflow boundary. The accuracy of metric coefficients should also be expected to decrease in this region. This situation would be improved by employing a more smoothly varying mesh geometry, but no attempt could be made in this direction in this work.

(b) Insufficient damping. Local instabilities around the critical regions could be damped by systematically increasing the various damping coefficients in the integration procedure. Implementation of other conservative smoothing or damping functions could also be tried. A comprehensive study in this direction is also beyond the scope of the present contract.

In figures 20-24 results for this case are shown just before the calculation goes unstable. The computation is not yet converged but the shock structure in the flow field is already established. In figure 20 the pressure distribution on the ramp surface for this case is compared with the pressure distribution obtained from the inviscid (Euler) calculations. The distributions are very similar except for the dip in the pressure observed in the viscous calculations close to the ramp leading edge. The same effect is observed in the calculations reported in reference 9. Pressure distributions on the cowl inner surface are shown in figure 21, whereas figure 22 displays pressure distributions on the cowl outer surface. In both cases the distributions obtained from the present calculations differ considerably from the inviscid distributions probably because the viscous solution is not yet converged. Density contours for this case are shown in figure 23, in which the ramp shock is clearly seen to converge on the cowl tip as expected from the design considerations. However, the flow

field around the cowl tip is not properly established at this point in the calculation. Finally in figure 24, the velocity and pressure distributions in the ramp boundary layer close to the inlet exit plane are shown. The velocity profile suggests that with the current grid a turbulent boundary layer develops on the ramp. As expected, the pressure stays constant across the boundary layer.

During portions of all of the computations reported above, in order to have numerical stability, we have found it necessary to keep the Courant number less than one. This requirement is equivalent to the Courant-Friedrichs-Lewy (CFL) condition which must be obeyed to bound the step size in the marching direction in explicit march techniques. This was true in spite of the fact that on the basis of linear stability analysis, in implicit schemes the CFL condition is expected to be relaxed so that the Courant number can assume values much larger than one.

If should be further noted that the approximate factorization algorithm used is only neutrally stable (ref. 4). Therefore, steady-state convergence cannot be accelerated by the use of very large time-steps, even where their use introduces no instability.

4. CONCLUDING REMARKS

A time-implicit finite-difference solution procedure for the Euler equations has been applied to the calculation of two-dimensional inlet flow fields. Results for a practical inlet configuration are presented. Results for supercritcal operation with uniform and non-uniform inflow conditions indicate that the solutions converge fairly rapidly for these cases; the accuracy of the method under these conditions, however, awaits experimental evaluation. Because the calculations have been performed using only one computational grid, grid refinement studies and an evaluation of the impact of the chosen

grid generation schemes on the computational accuracy should also be made. Calculations performed for a subcritical case have indicated that for this case the solution converges very slowly. The necessity of using a special smoothing operator as well as very small time-steps are contributing factors.

Calculations performed using the same method for the Navier-Stokes equations with the thin-layer approximation indicate that convergence of the calculation is also very slow for this case. To alleviate numerical instabilities that occur in some critical portions of the flow field, it appears that the Courant number must be kept much less than one, at least until the flow field is established in those regions. The necessity of having to keep the Courant number less than one in a variety of cases and the neutral stability of the solution scheme used diminishes the advantage of using the implicit method. Hence, the extra computational effort of block tridiagonal matrix inversion associated with the implicit method does not seem worthwhile. It is our belief that unless the stability properties of implicit methods are improved, for the class of problem studied here, space-marching methods for supercritical flows or explicit time-marching methods will provide a less expensive alternative.

Before this method is considered for use either as a design tool in its present two-dimensional form or for extension to three dimensions, its convergence properties for subcritical cases and for cases calculated including viscous effects need substantial improvement. Additionally, further work is needed to understand the sources of the numerical instabilities encountered during the viscous calculations reported herein.

REFERENCES

1. Chaussee, D. S. and McMillan, O. J.: A Supersonic, Three-Dimensional Code for Flow Over Blunt Bodies - User's Manual, NASA CR-3223, January 1980.

2. Chaussee, D. S. and McMillan, O. J.: A Supersonic Three-Dimensional Flow Over Blunt Bodies - Program Documentation and Test Cases. NASA CR-3224, February 1980.

3. Beam, R. and Warming, R. F.: An Implicit Finite-Difference Algorithm for Hyperbolic Systems in Conservation-Law Form. J. Comp. Physics, vol. 22, September 1976, pp. 87-110.

4. Steger, J. L.: Implicit Finite Difference Simulation of Flow About Arbitrary Geometries with Application to Airfoils. AIAA Paper No. 77-665, June 1977.

5. D'Souza, N., Moulder, S., and Moretti, G.: Numerical Method for Hypersonic Internal Flow Over Blunt Leading Edges and Two Blunt Bodies. AIAA Journal, vol. 10, no. 5, May 1972.

6. Bansod, P.: Supersonic Flow About Ducted Bodies with Subsonic Internal Boundaries. AIAA Journal, vol. 12, no 5, May 1972.

7. Knight, D. D.: Numerical Simulation of Realistic High-speed Inlets Using the Navier-Stokes Equations. AIAA Journal, vol. 15, no. 11, November 1977.

8. Presley, L. L.: Internal Flow Calculations for Axisymmetric Supersonic Inlets at Angle of Attack, AIAA Paper-1214, Anaheim, 1975.

9. Buggeln, R. C., McDonald, H., Levy, R., and Kreskovsky, J. P.: Development of a 3-D Supersonic Inlet Flow Analysis. NASA CR-3218, January 1980.

10. Fuller, D. E.: Pressure Distributions for a Rectangular Supersonic Inlet at Subsonic Speeds. NASA TM X-3305, 1976.

11. Biringen, S. and McMillan, O. J.: Calculation of Two-Dimensional Inlet Flow Fields by an Implicit Method Including Viscous Effects - Program Documentation and Test Cases. NASA CR-3414, 1981.

12. Biringen, S. and McMillan, O. J.: Calculation of Two-Dimensional Inlet Flow Fields by an Implicit Method Including Viscous Effects - User's Manual. NASA CR-3412, 1981.

13. Sorenson, R. L. and Steger, J. L.: Simplified Clustering of Nonorthogonal Grids Generated by Elliptic Partial Differential Equations. NASA TM-73252, August 1977.

14. Thames, F. C., Thompson, J. F. and Mastin, C. W.: Numerical Solution of the Navier-Stokes Equations of Arbitrary Two-Dimensional Airfoils. NASA SP-347, 1975, Pt. 1, pp. 569-530.

15. Tannehill, J. C., Holst, T. C. and Rakich, J. V.: Numerical Computation of Two-Dimensional Viscous Blunt Body Flows With an Impinging Shock. AIAA Journal, vol. 14, February 1976.

16. MacCormack, R. W. and Lomax, H.: Numerical Solution of Compressible Viscous Flows. Ann. Rev. Fluid Mech., vol. 11, p. 289, 1979.

17. Baldwin, B. S. and Lomax, H.: Thin-Layer Approximation and Algebraic Model for Separated Flows. AIAA Paper No. 78-257, January 1978.

18. Beam, R. and Warming, R. F.: An Implicit Factored Scheme for the Compressible Navier-Stokes Equations. AIAA Paper No. 77-645, June 1977.

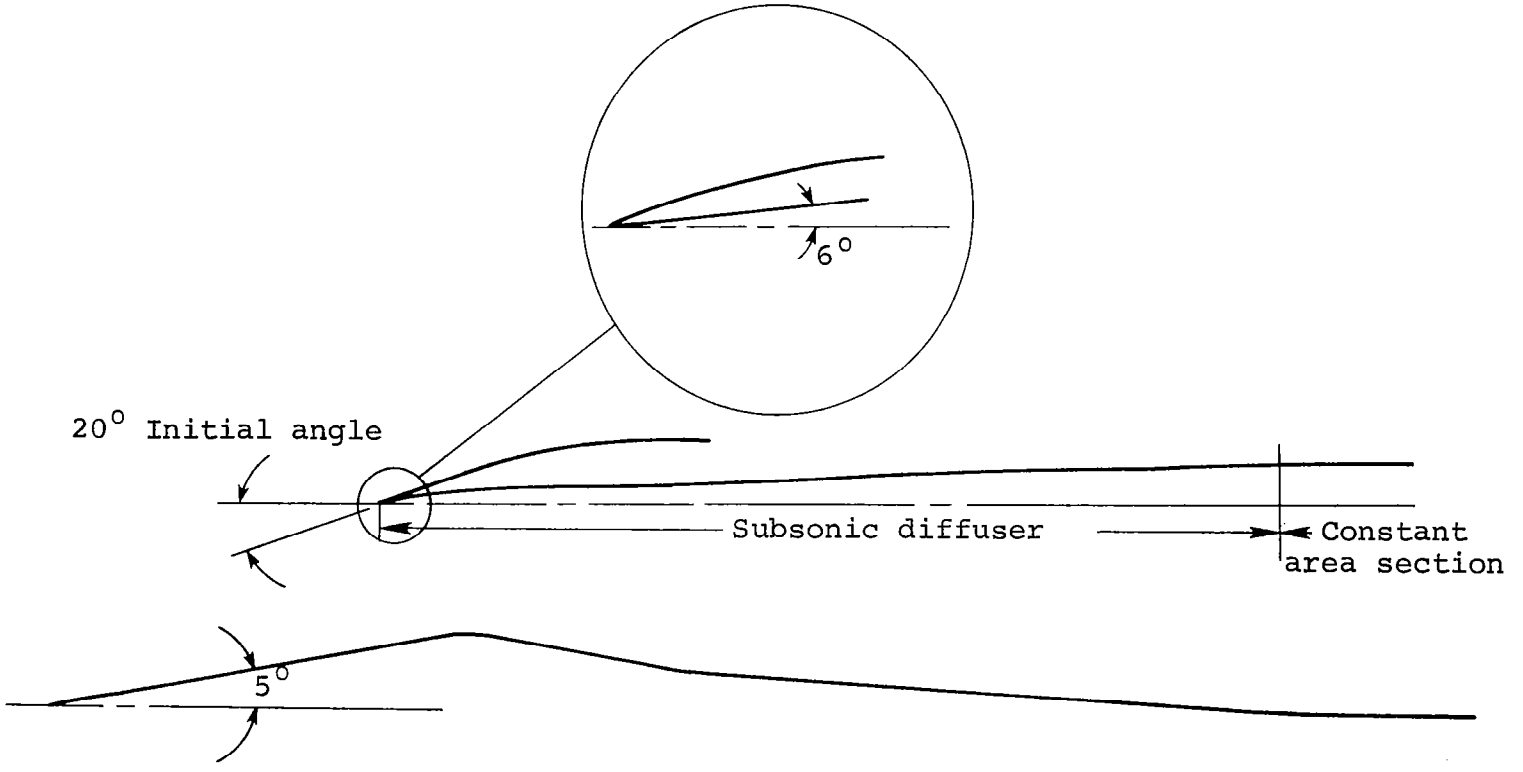

Figure 1.- Schematic of inlet geometry, design Mach number of 3.5.

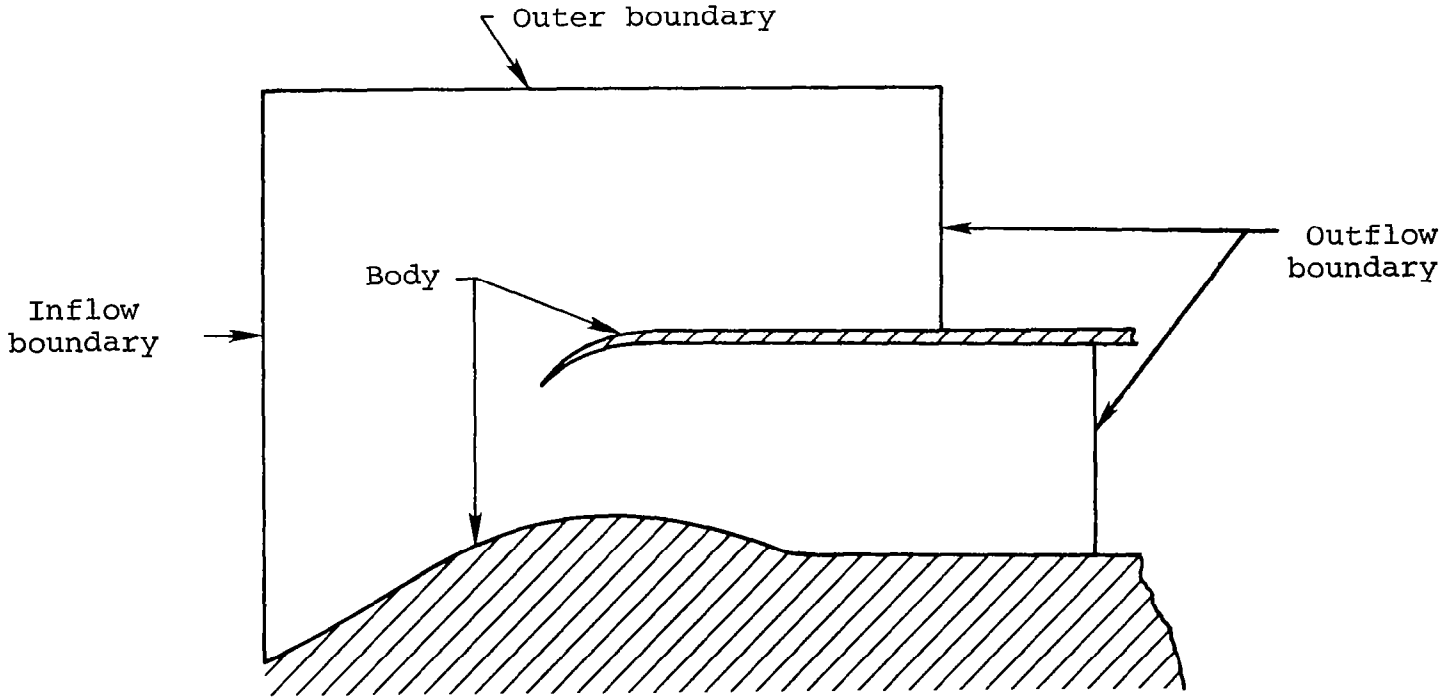

Figure 2.- Flow-field boundaries.

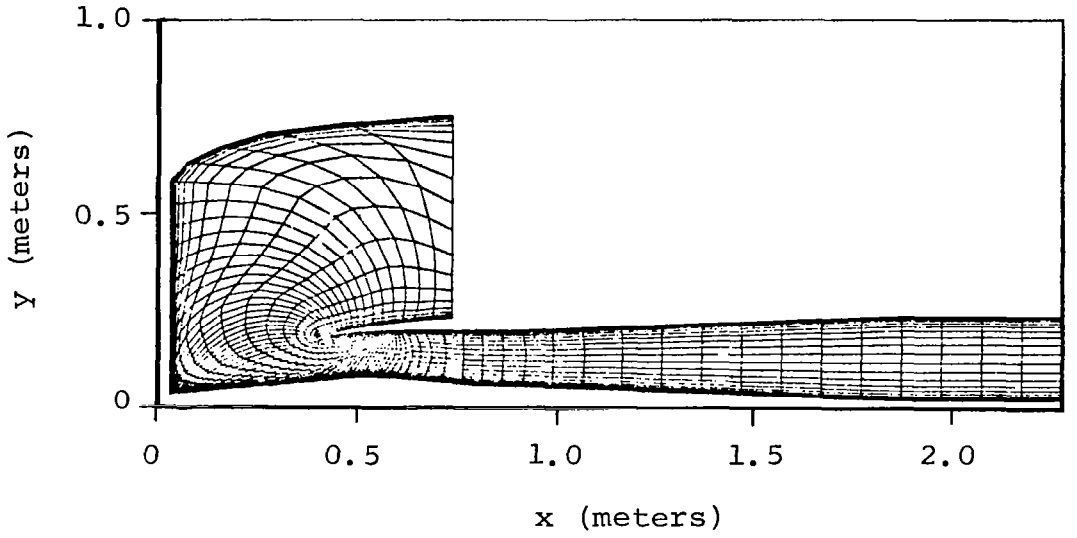

Figure 3.- Grid system used in the inviscid calculations.

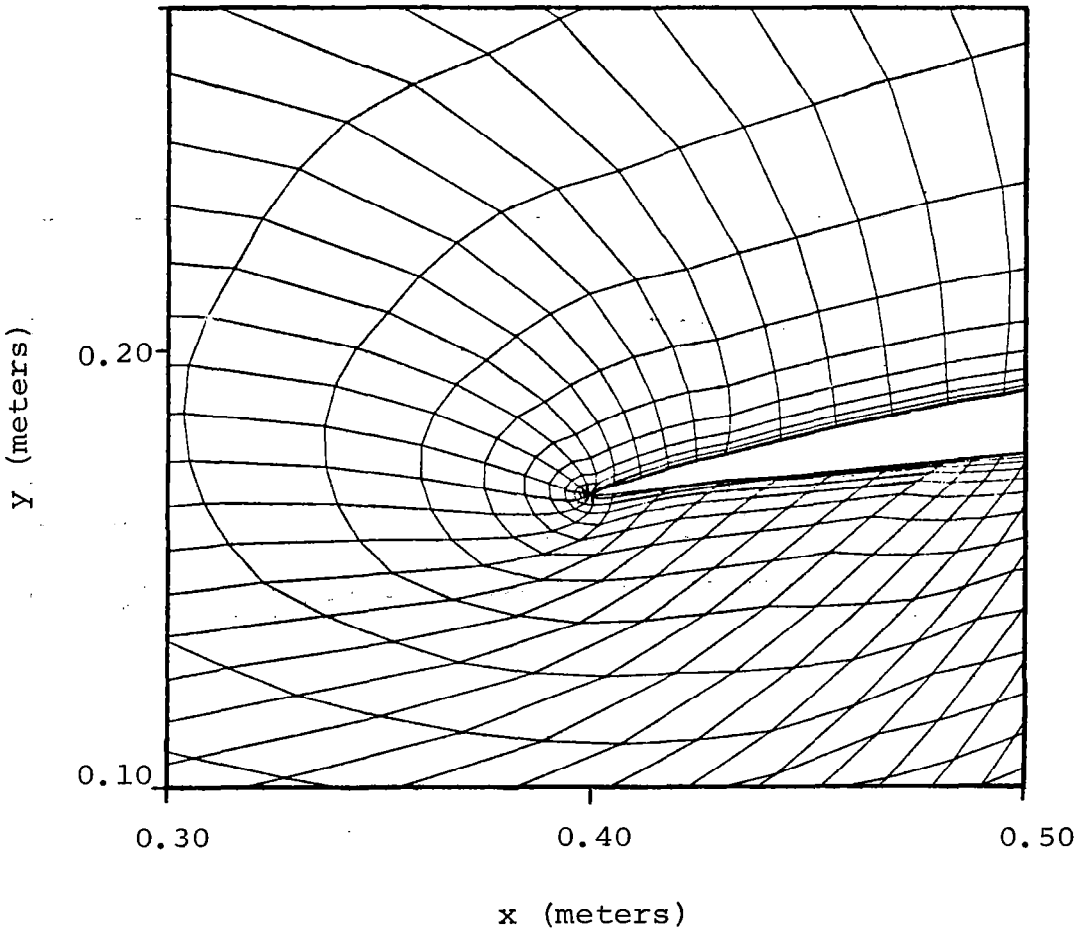

Figure 4.- Details of the grid in the vicinity of the cowl tip.

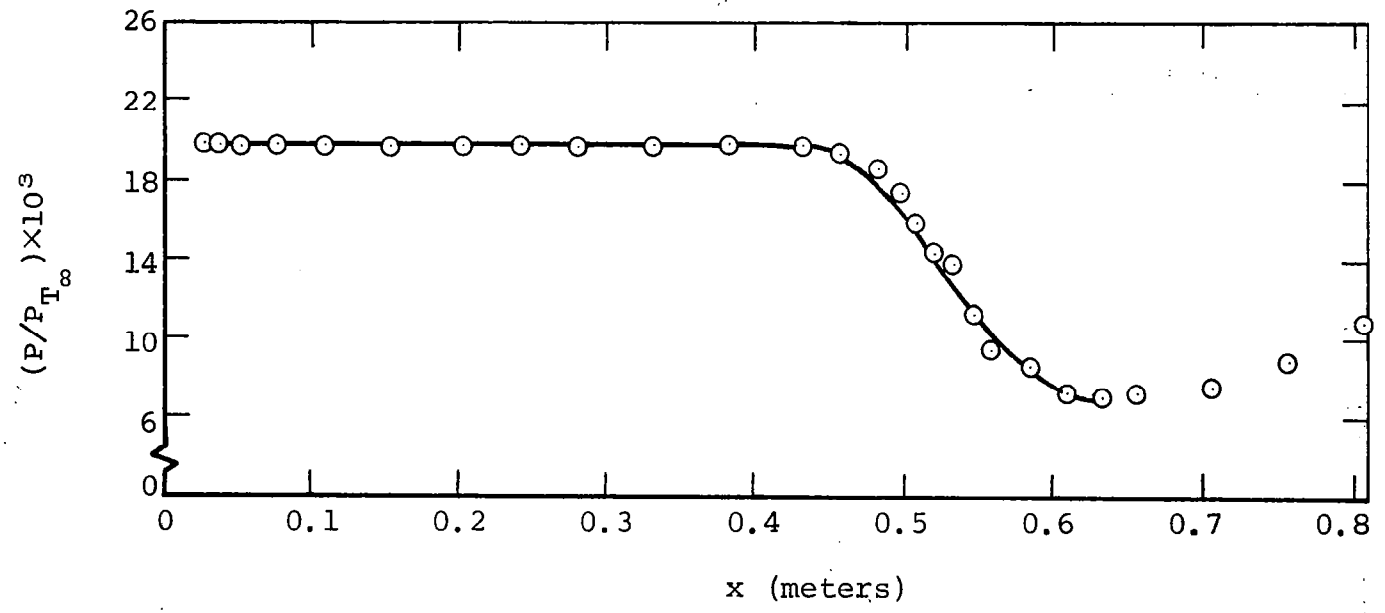

Figure 5.- Pressure distribution on ramp surface, supercritical flow; ⊙, computation; _____; shock-expansion theory.

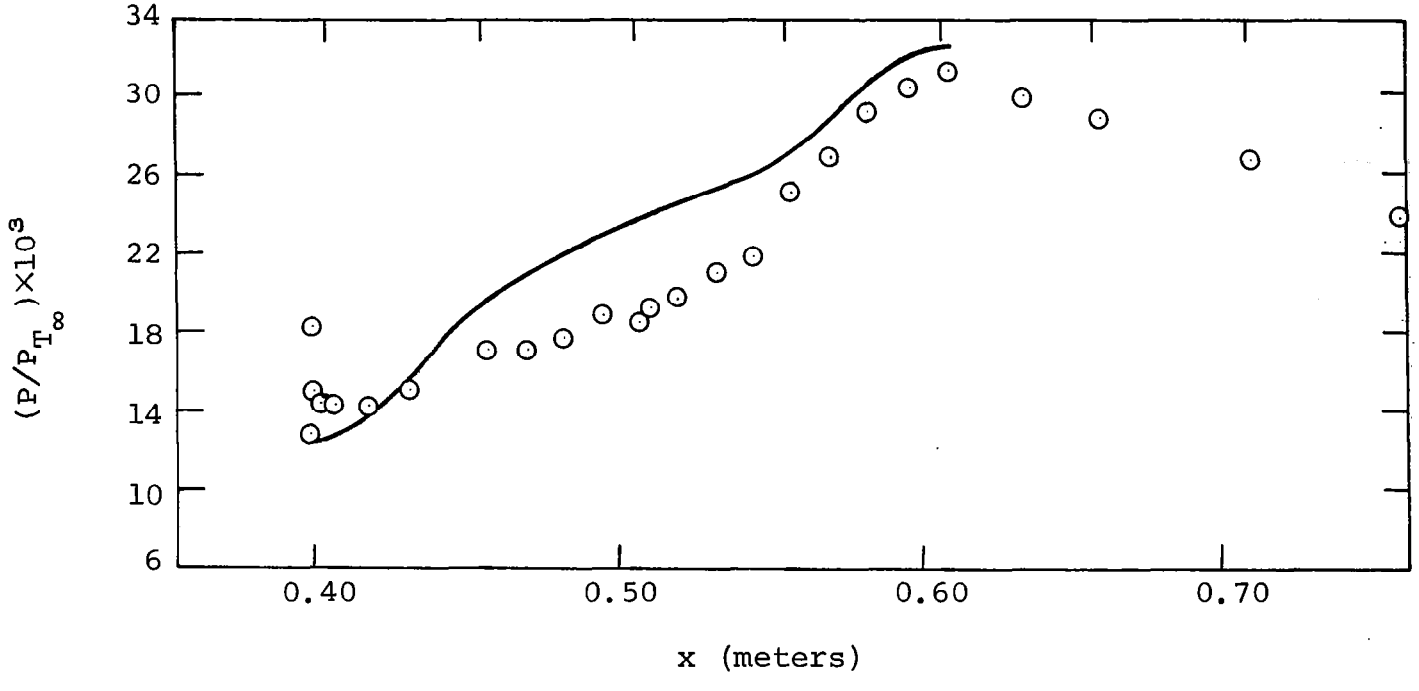

Figure 6.- Pressure distribution on cowl inner surface supercritical flow; ⊙, computation; _____; shock-expansion theory.

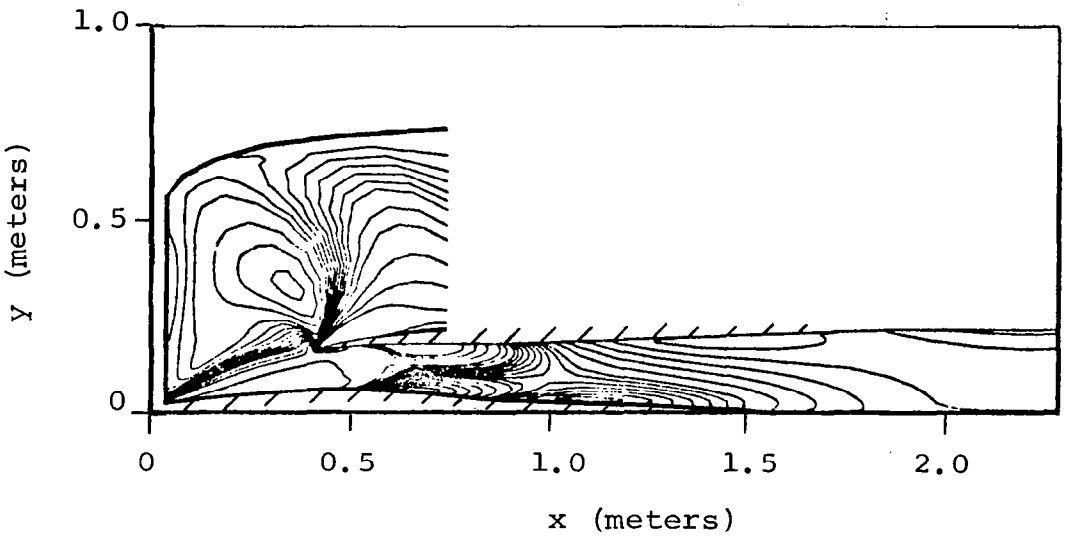

M_∞ = 3.50 α = 0.00

Figure 7.- Pressure contours, supercritical case.

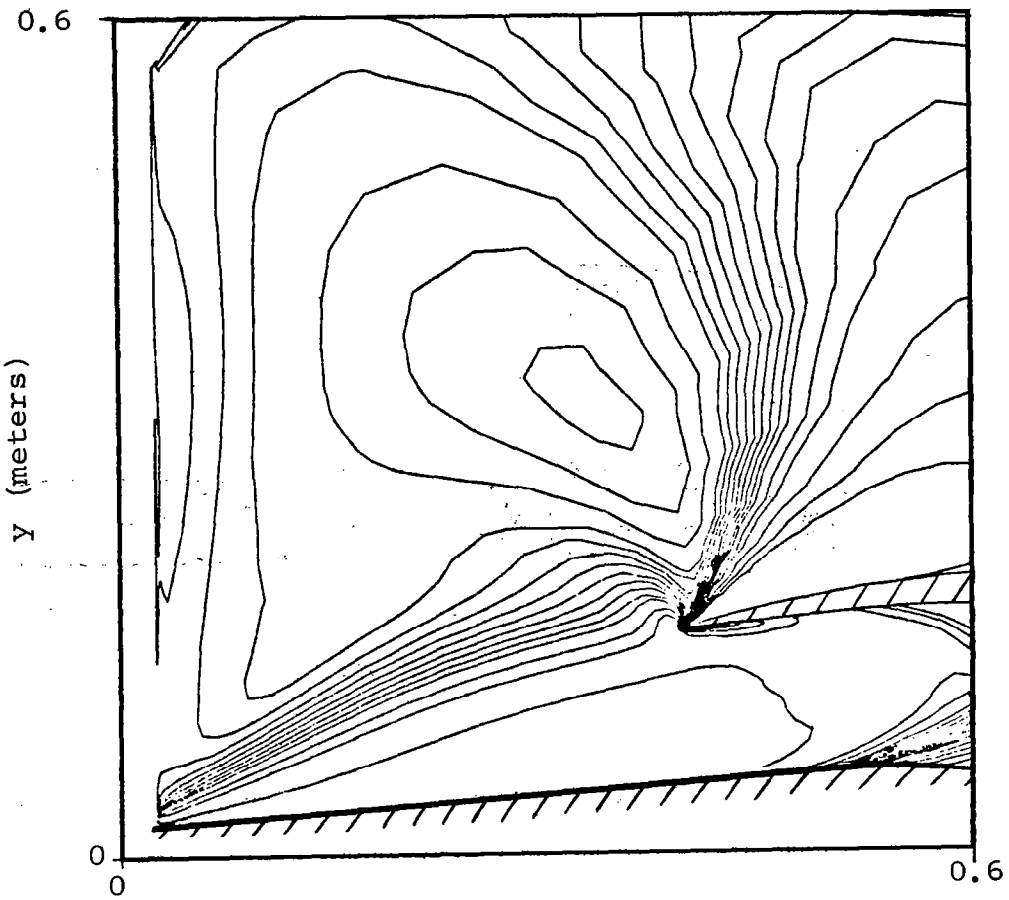

$M_\infty = 3.50$ $\alpha = 0.0$

Figure 8.- Details of pressure contours in the vicinity of cowl tip, supercritical case.

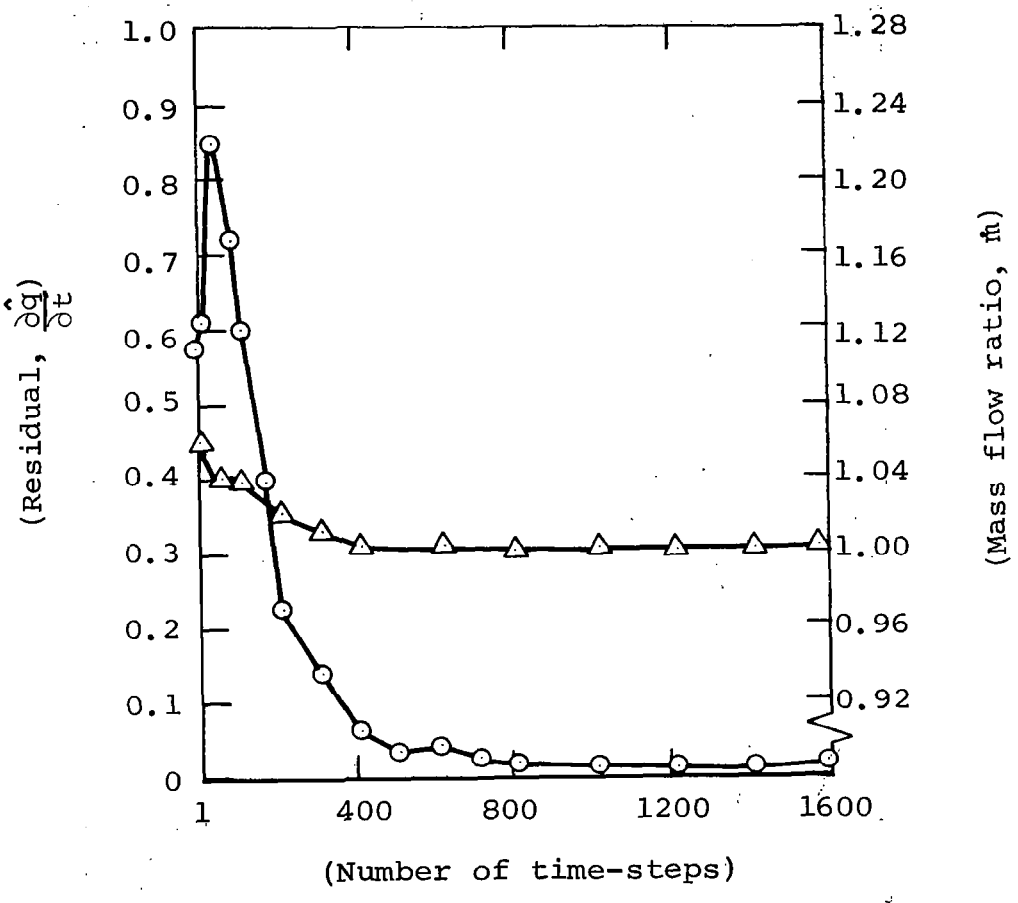

Figure 9.- Rate of convergence of the supercritical solution; ⊙, the residual; △, $\dot{m}$, mass flow ratio.

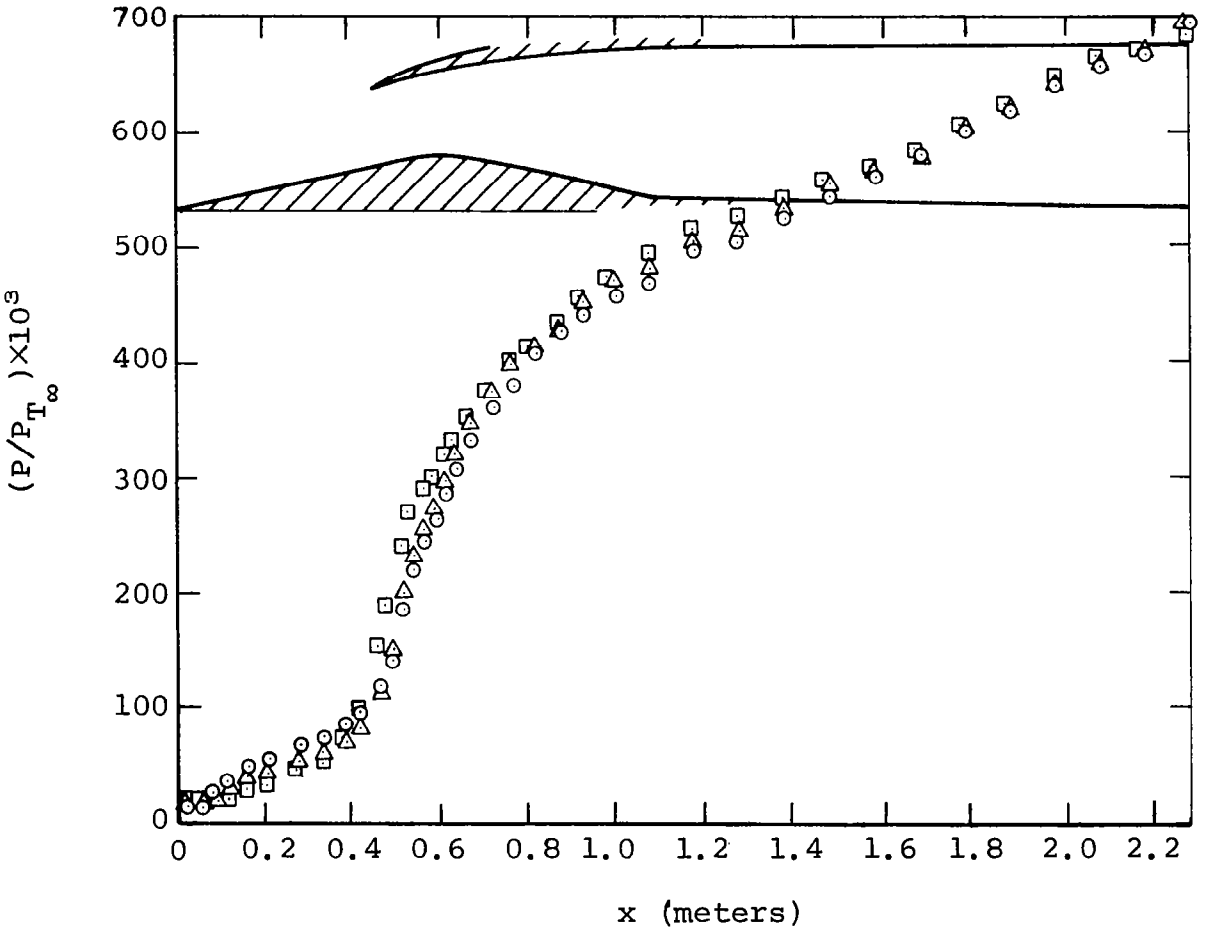

Figure 10,- Pressure distribution on ramp surface for subcritical solution with P_B/P_{T_∞} = 0.7; ⊙, at 7500 T.S.; △, at 8000 T.S.; □, at 8500 T.S.

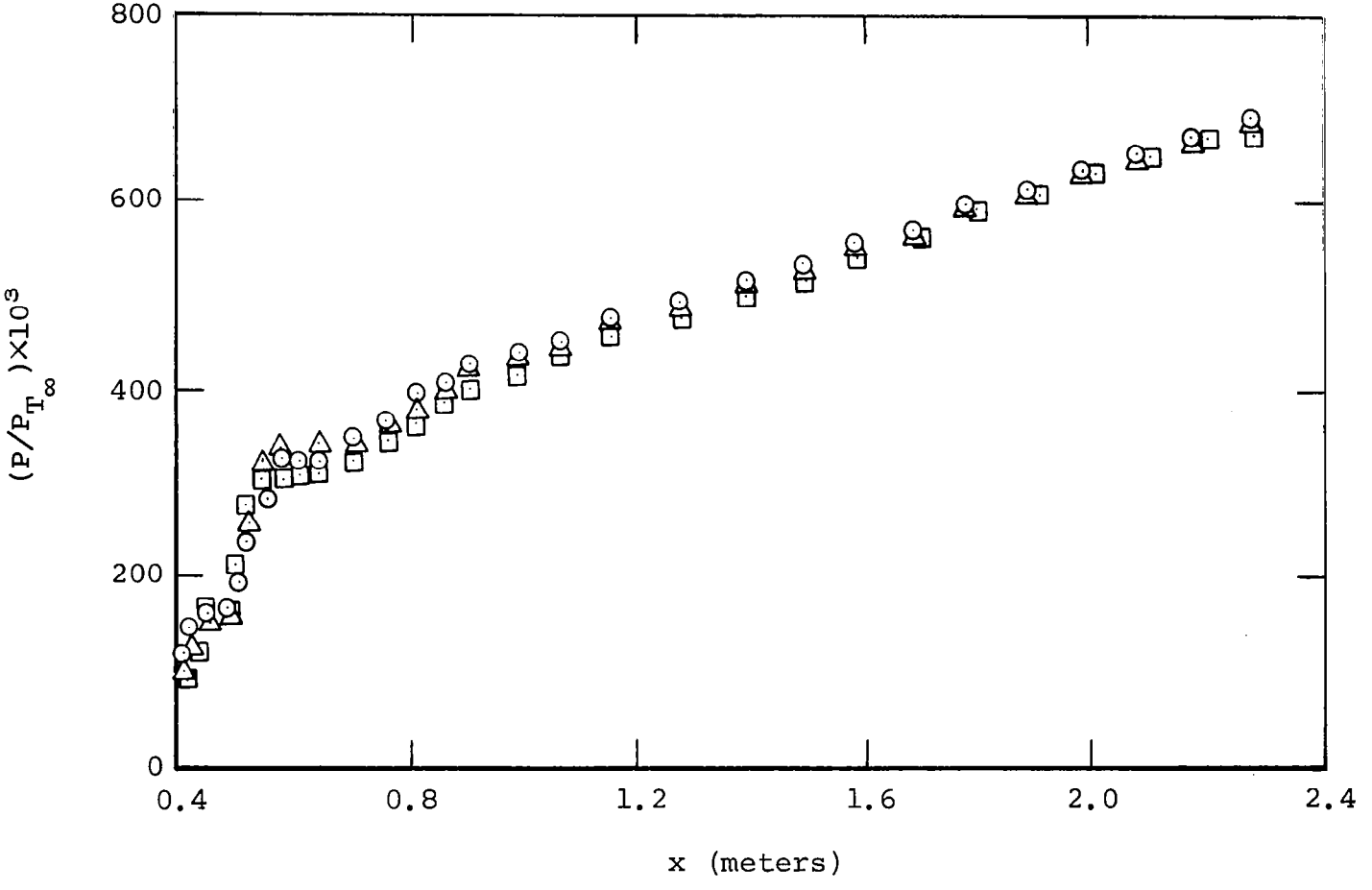

Figure 11.- Pressure distribution on cowl inner surface for subcritical solution with P_B/P_{T_∞} = 0.7; symbols as in figure 10.

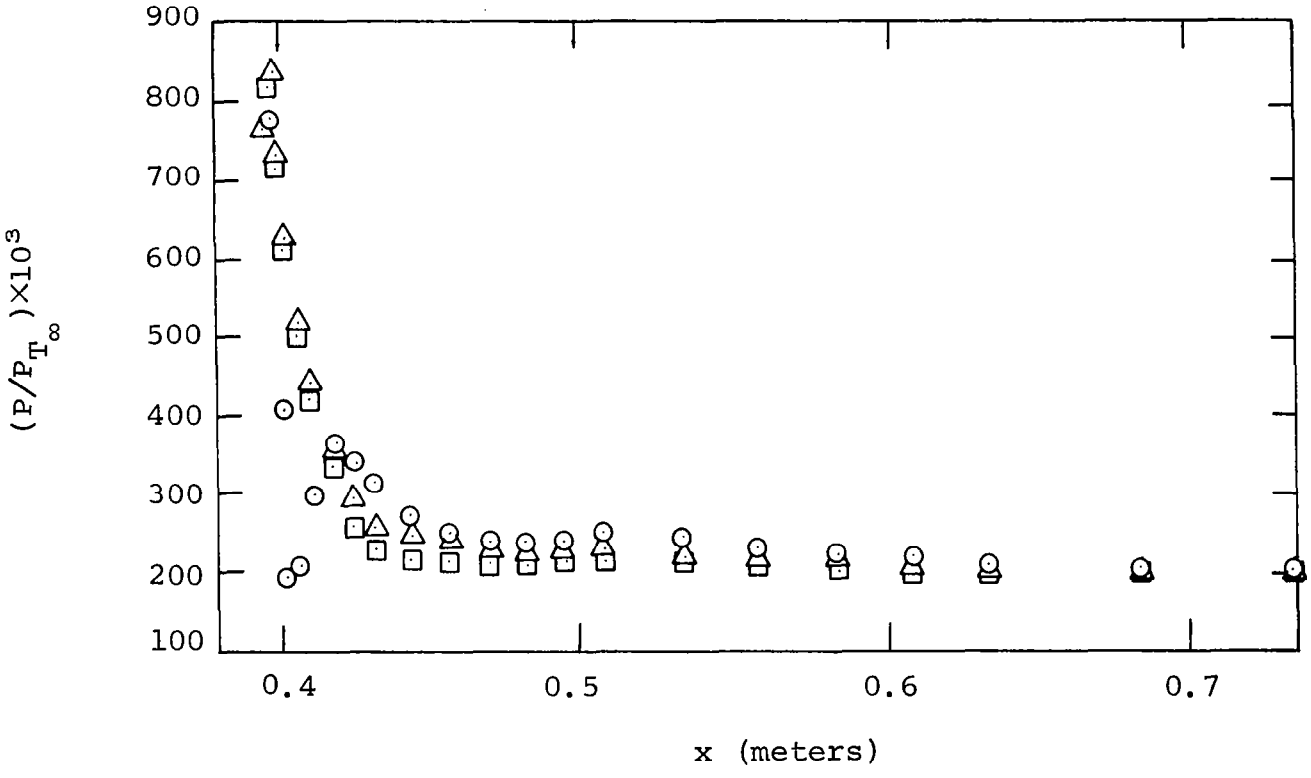

Figure 12.- Pressure distribution on cowl outer surface; subcritical solution with $P_B/P_{T_\infty} = 0.7$; symbols as in figure 10.

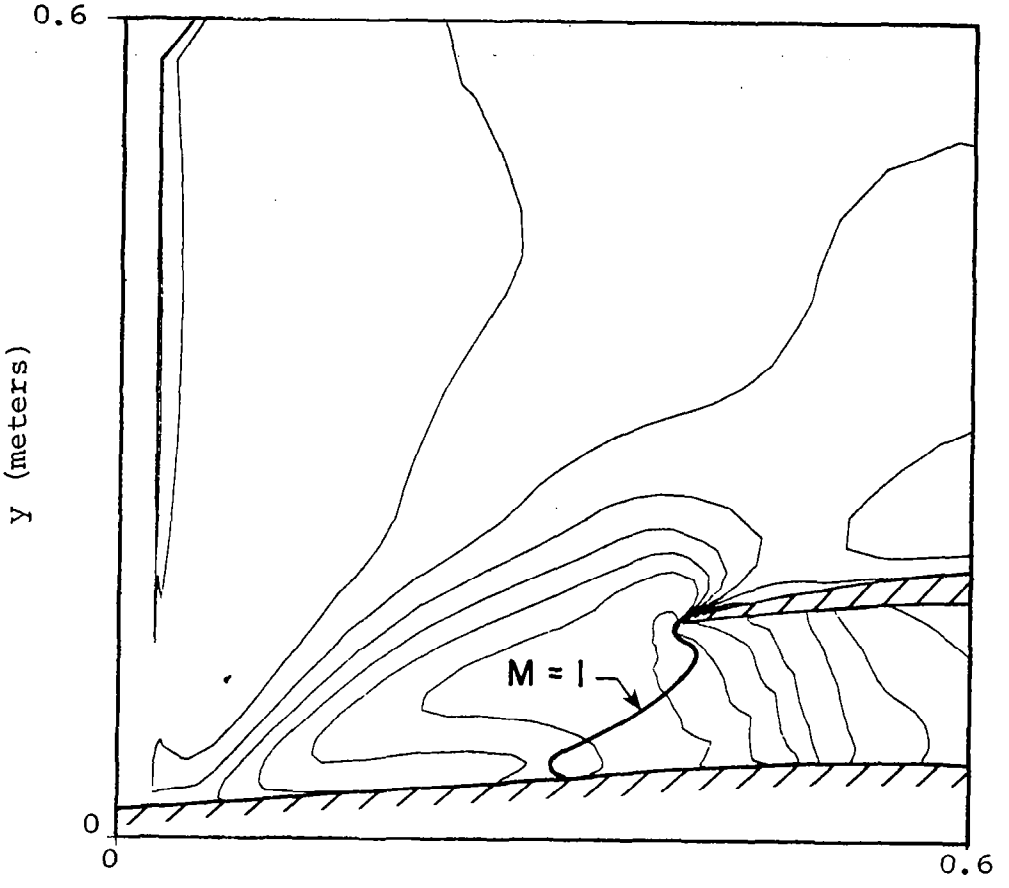

$M_\infty = 3.50 \qquad \alpha = 0.0$

Figure 13.- Details of density contours, subcritical case.

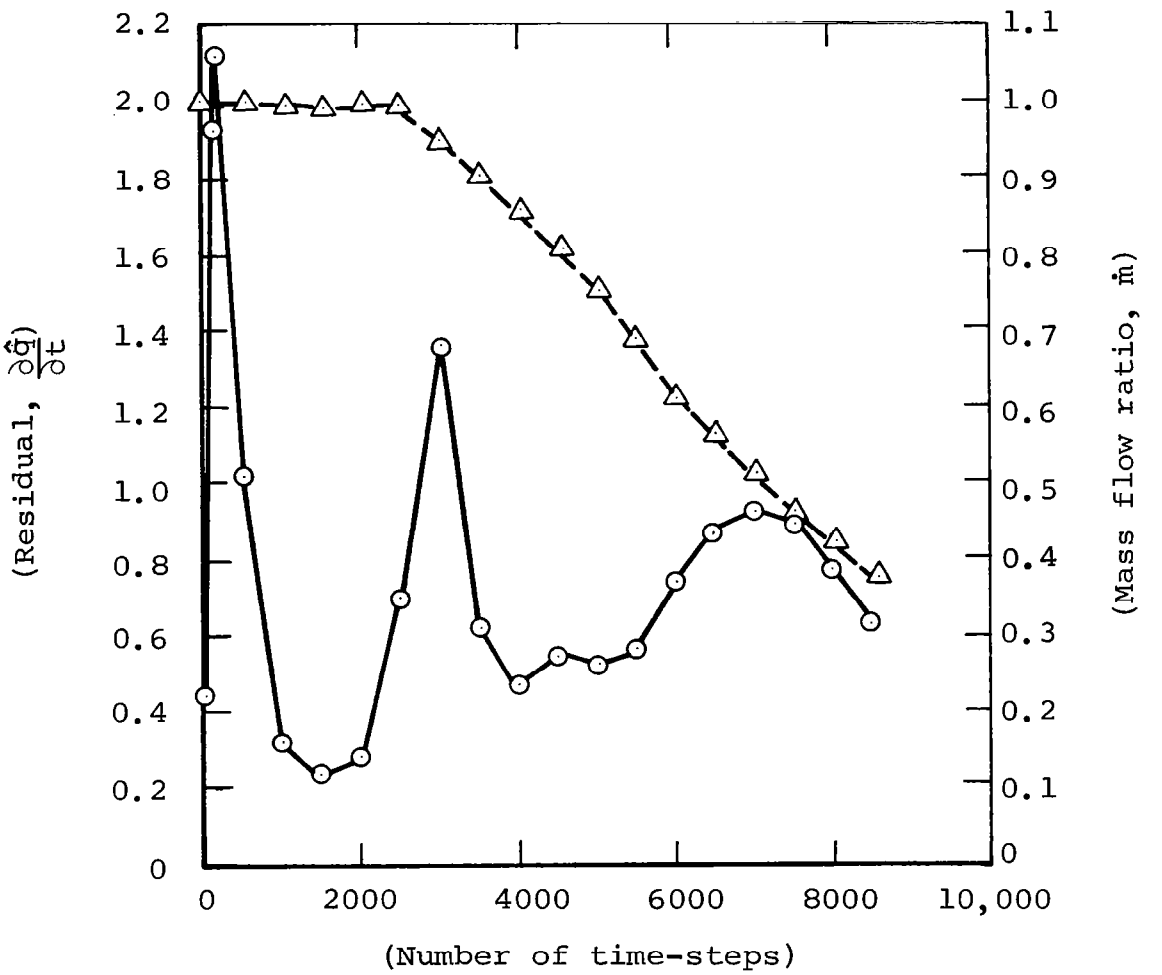

Figure 14.- Rate of convergence of the subcritical solution; ⊙, residual; △, $\dot{m}$, mass flow ratio.

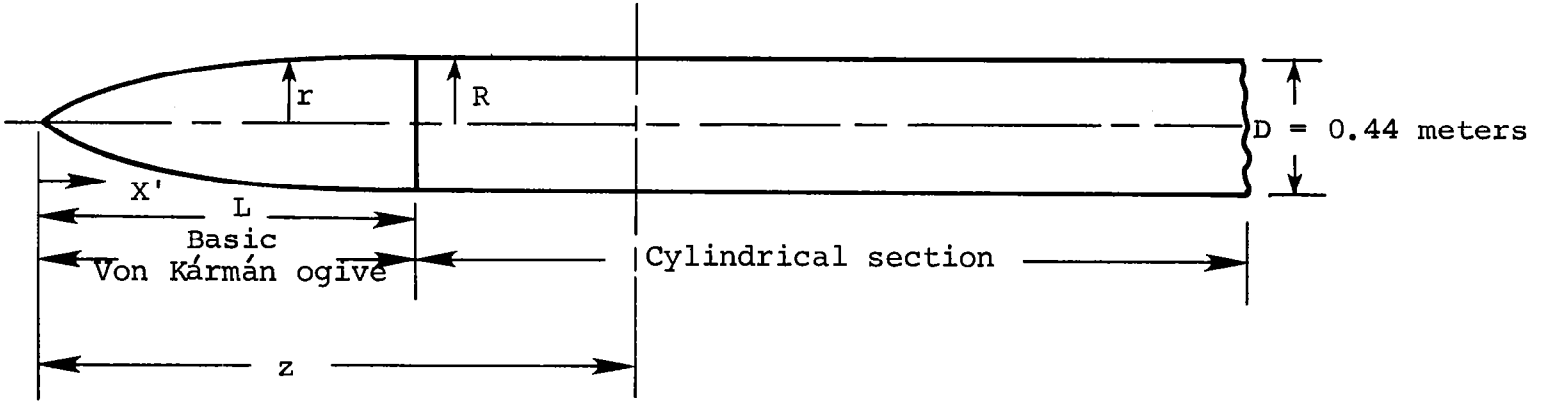

Von Kármán Ogive Nose

$$\frac{r}{R} = \frac{1}{\sqrt{\pi}} \sqrt{\psi - \frac{1}{2} \text{SIN } 2\psi}$$

$$\psi = \cos^{-1} \left(1 - 2\frac{X'}{L}\right)$$

$$0 \leq \frac{X'}{D} \leq 2.46$$

F = Fineness ratio = 2.46

D = Maximum body diameter

Cylindrical Section

$$\frac{r}{D} = 0.5$$

$$z = \left\{\begin{matrix}\text{Position of inlet} \\ \text{ramp leading edge}\end{matrix}\right\} = 4.5\ D$$

Figure 15.- Schematic of the forebody.

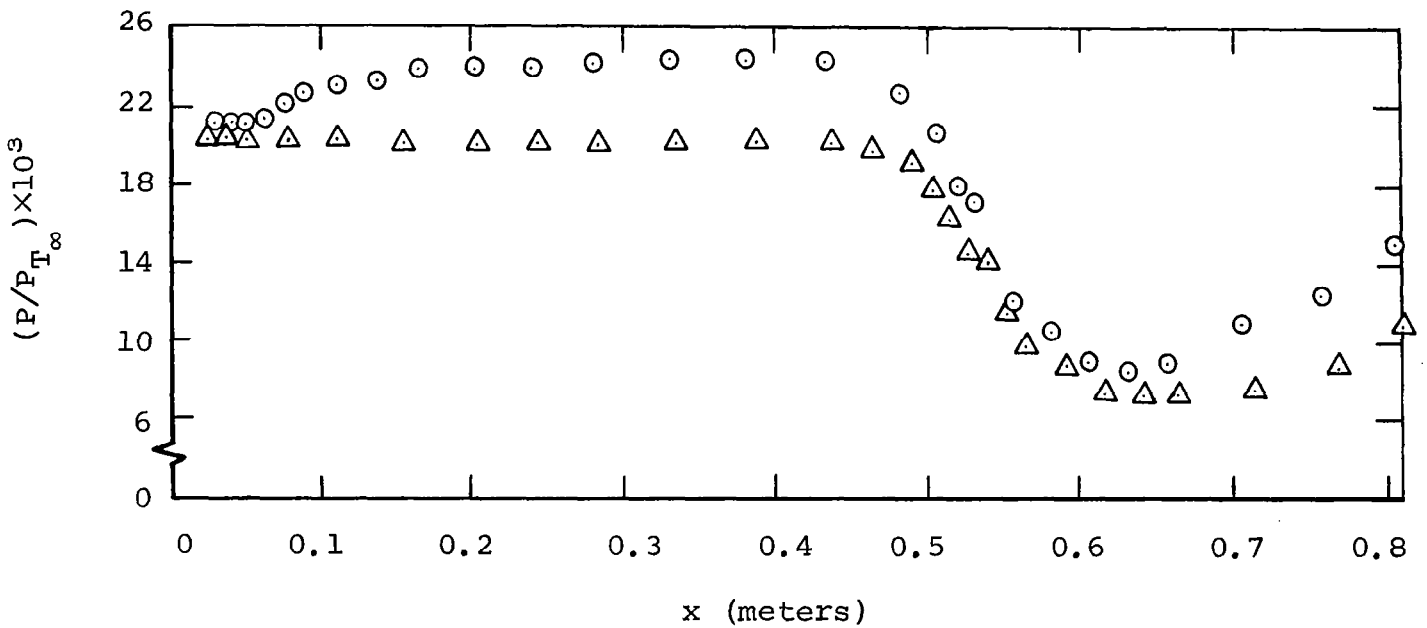

Figure 16.- Pressure distribution on ramp surface, supercritical flow results; ⊙, nonuniform initial conditions; △, uniform initial conditions.

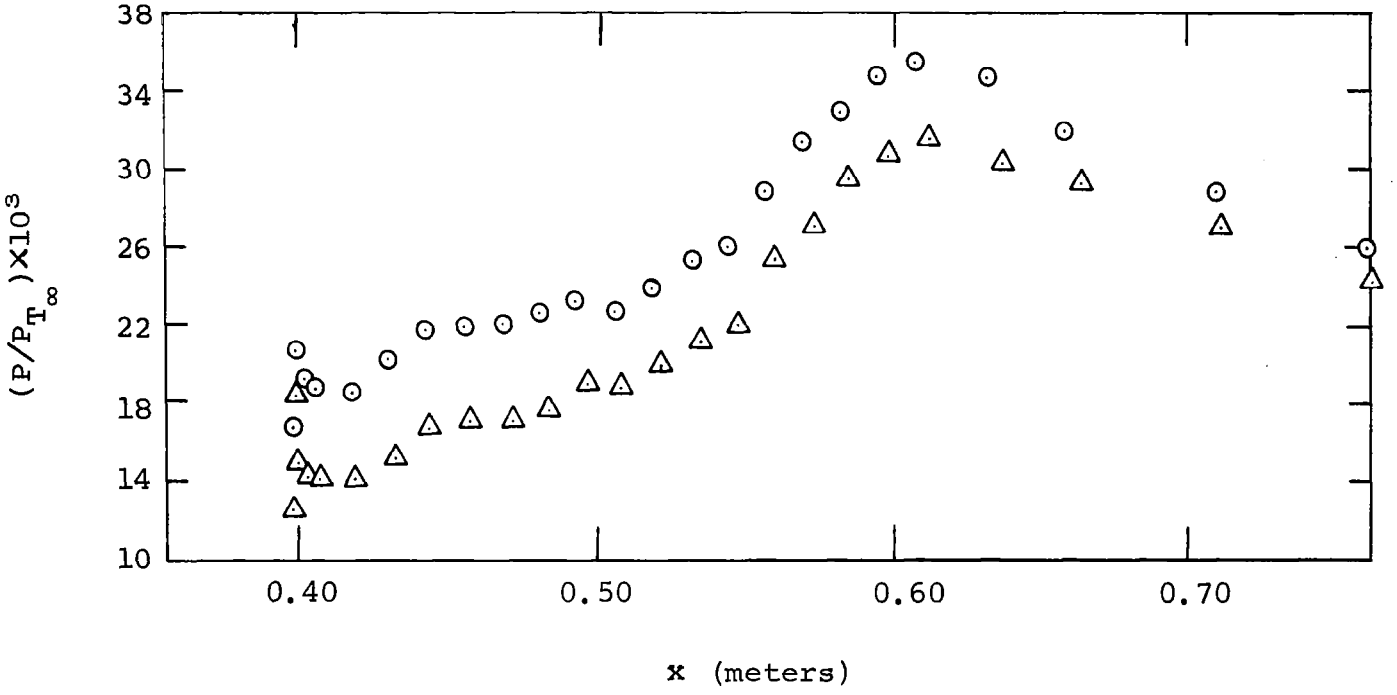

Figure 17.- Pressure distribution on cowl inner surface, supercritical flow results; ⊙, nonuniform initial conditions; △, uniform initial conditions.

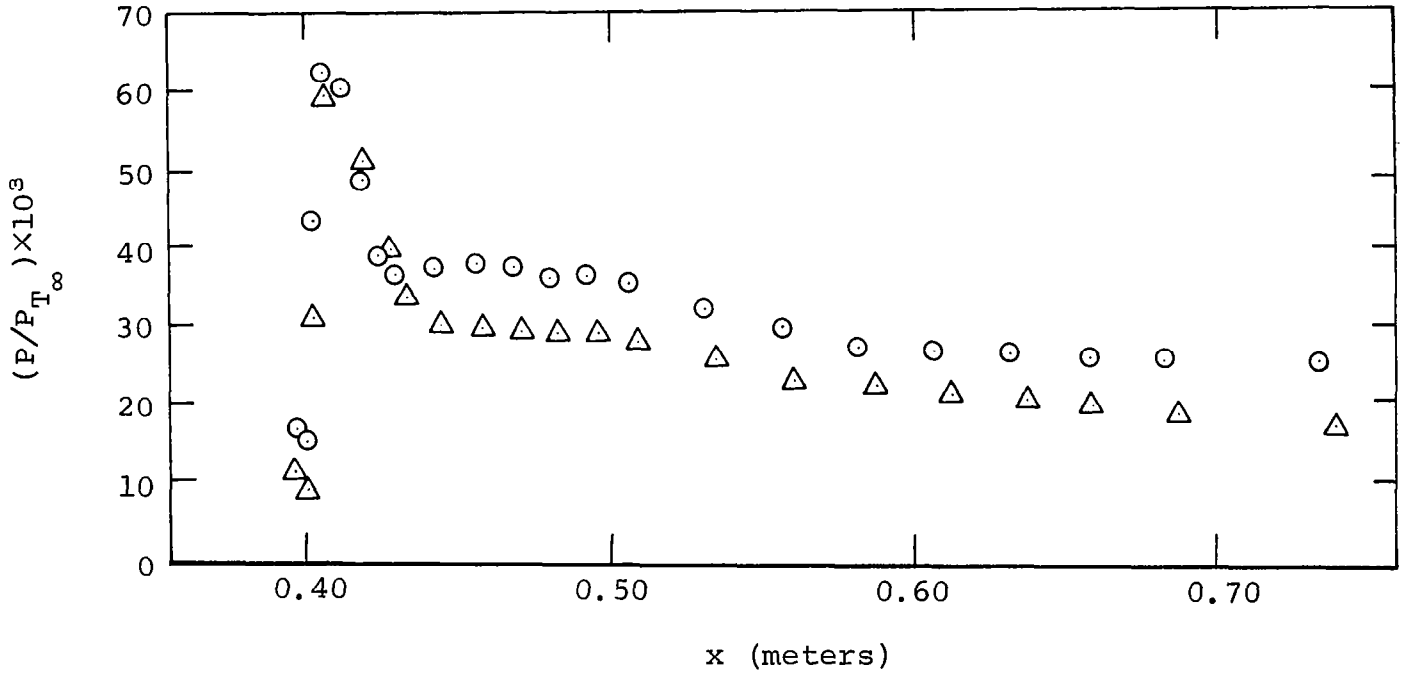

Figure 18.- Pressure distribution on cowl outer surface, supercritical flow results; ⊙, nonuniform initial conditions; △, uniform initial conditions.

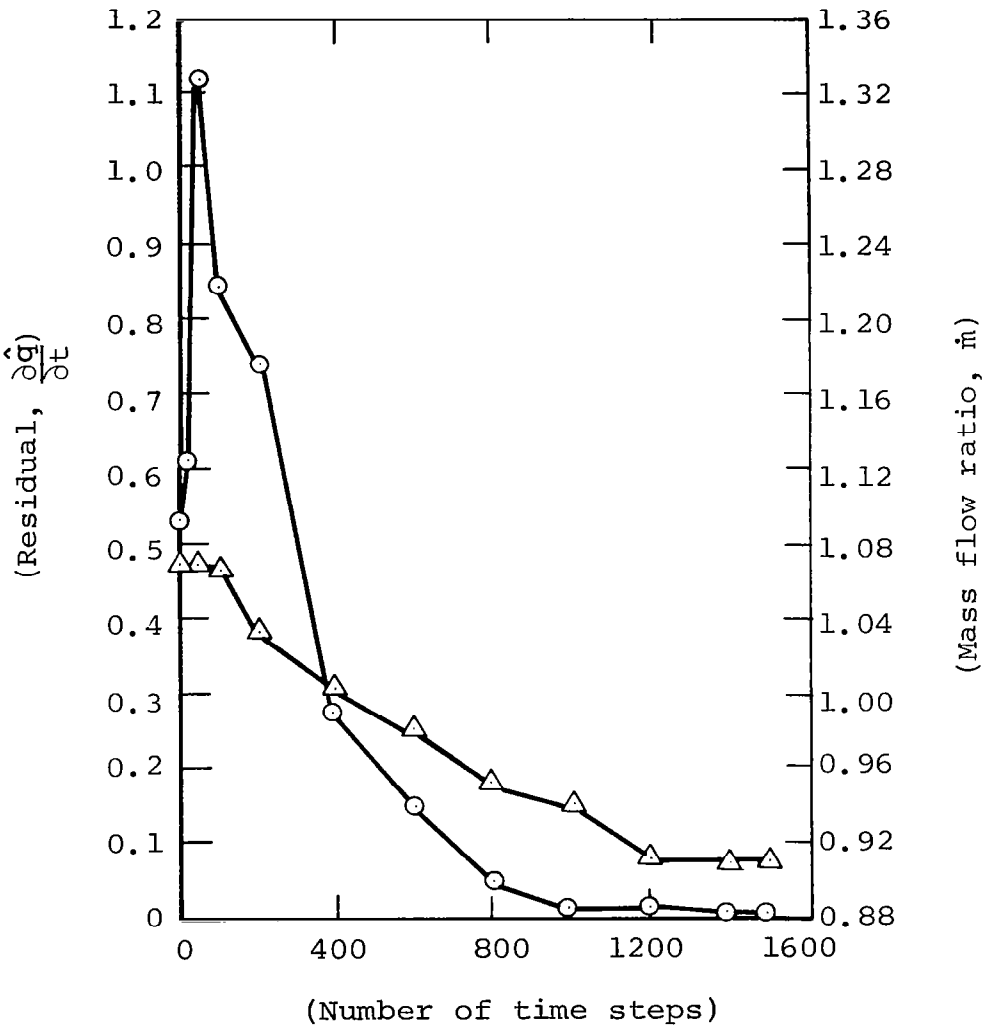

Figure 19.- Rate of convergence of supercritical solution with nonuniform initial conditions; ⊙, the residual; △, $\dot{m}$, the mass flow ratio.

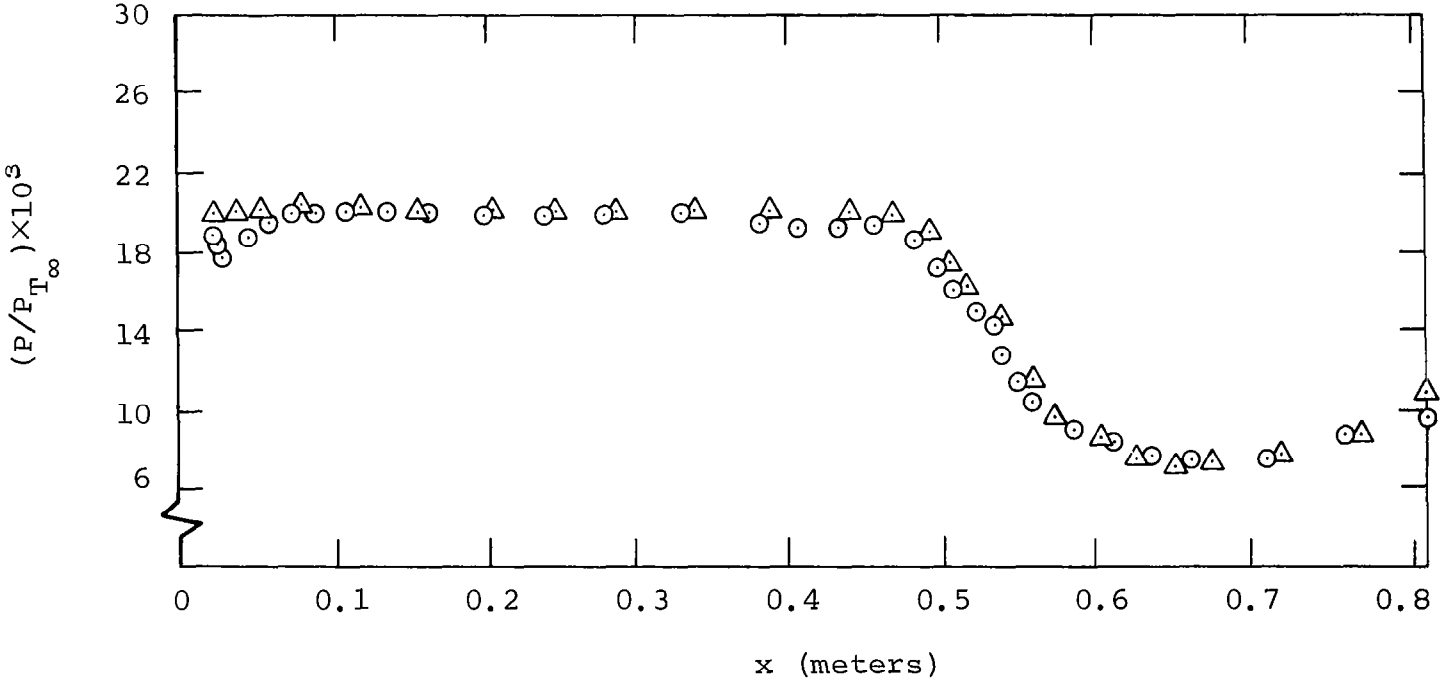

Figure 20.- Pressure distribution on ramp surface; ⊙, viscous calculations; △, inviscid calculations.

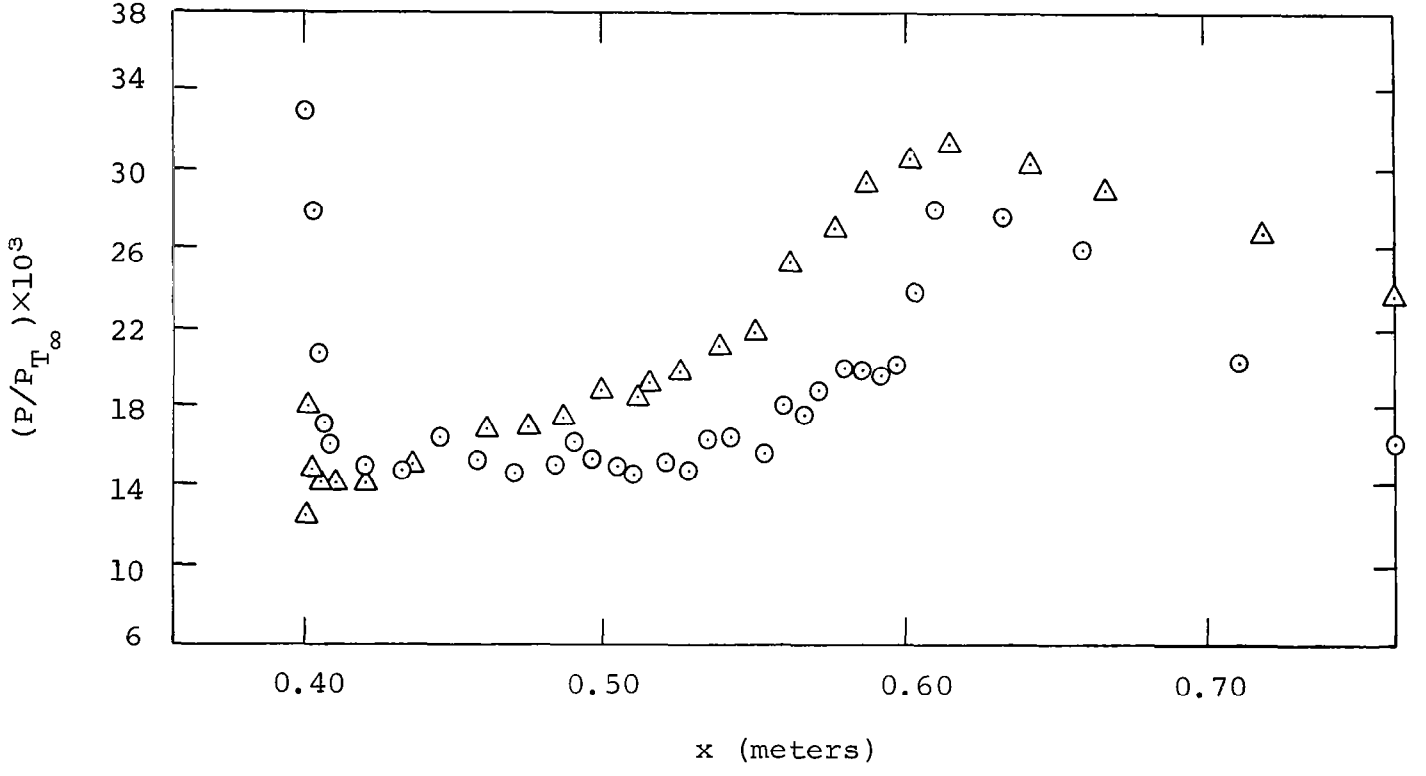

Figure 21.- Pressure distribution on cowl surface; ⊙, viscous calculations; △, inviscid calculations.

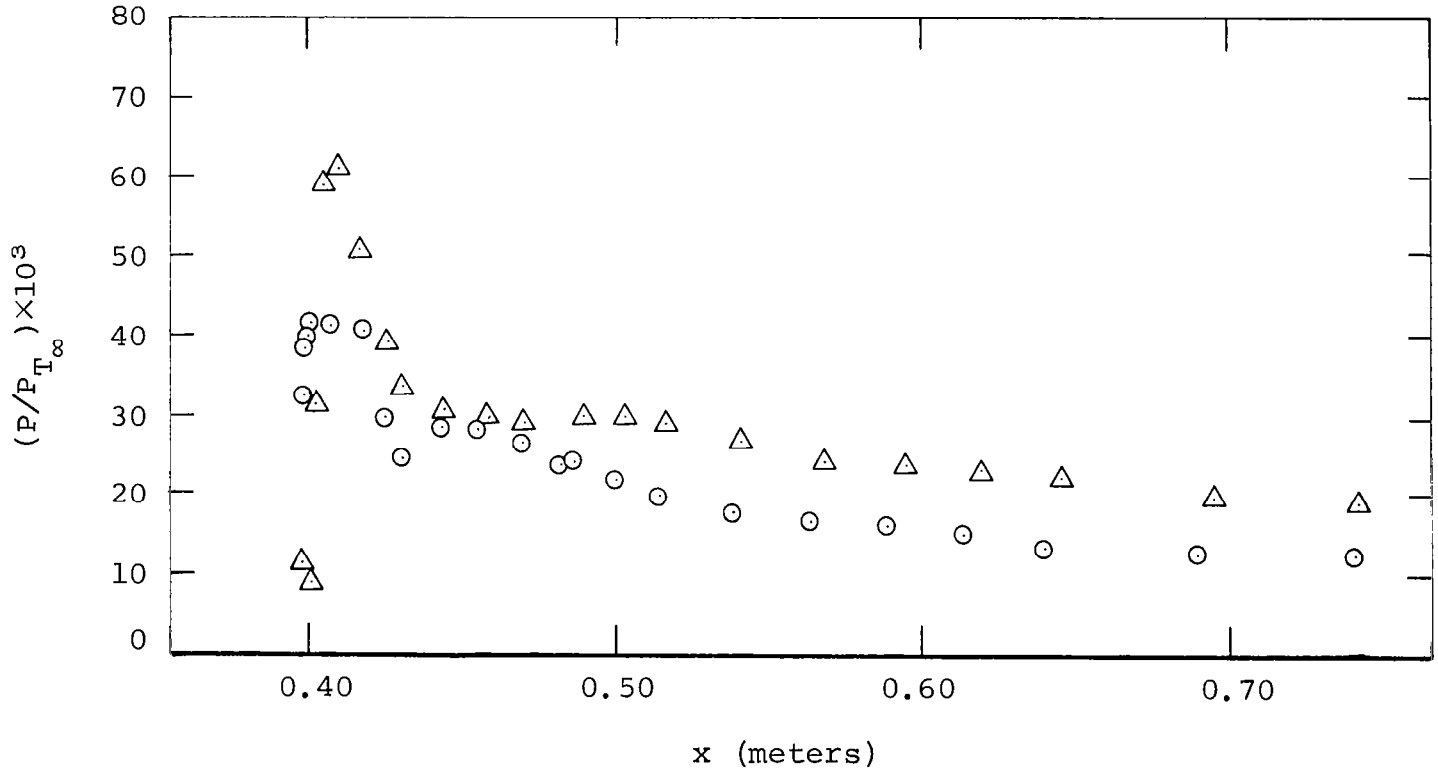

Figure 22.- Pressure distribution on cowl outer surface; ⊙, viscous calculations; △, inviscid calculations.

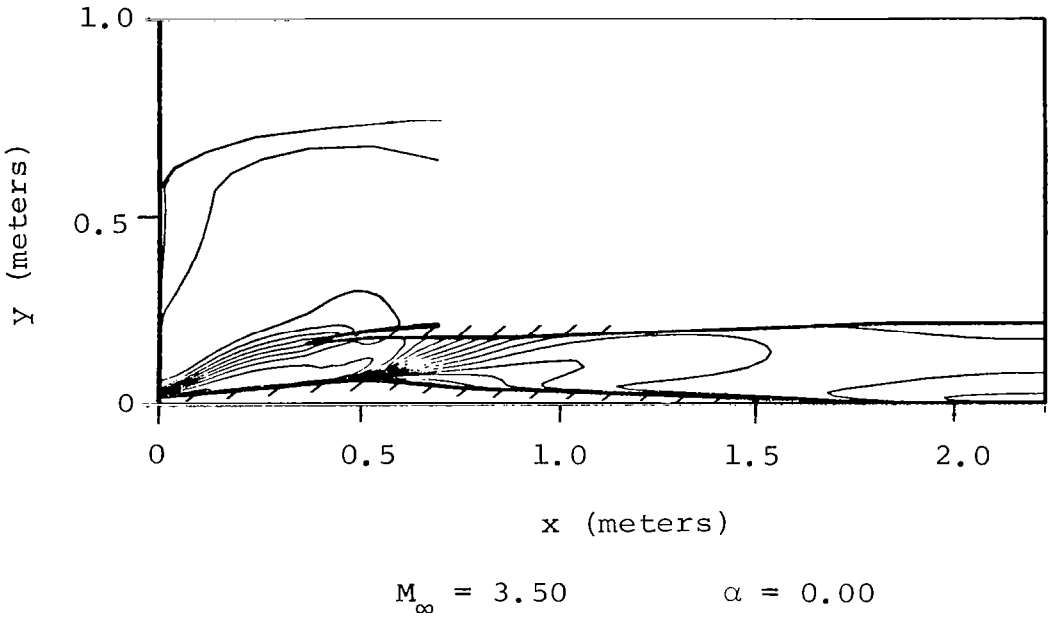

Figure 23.- Density contours; supercritical case, turbulent flow.

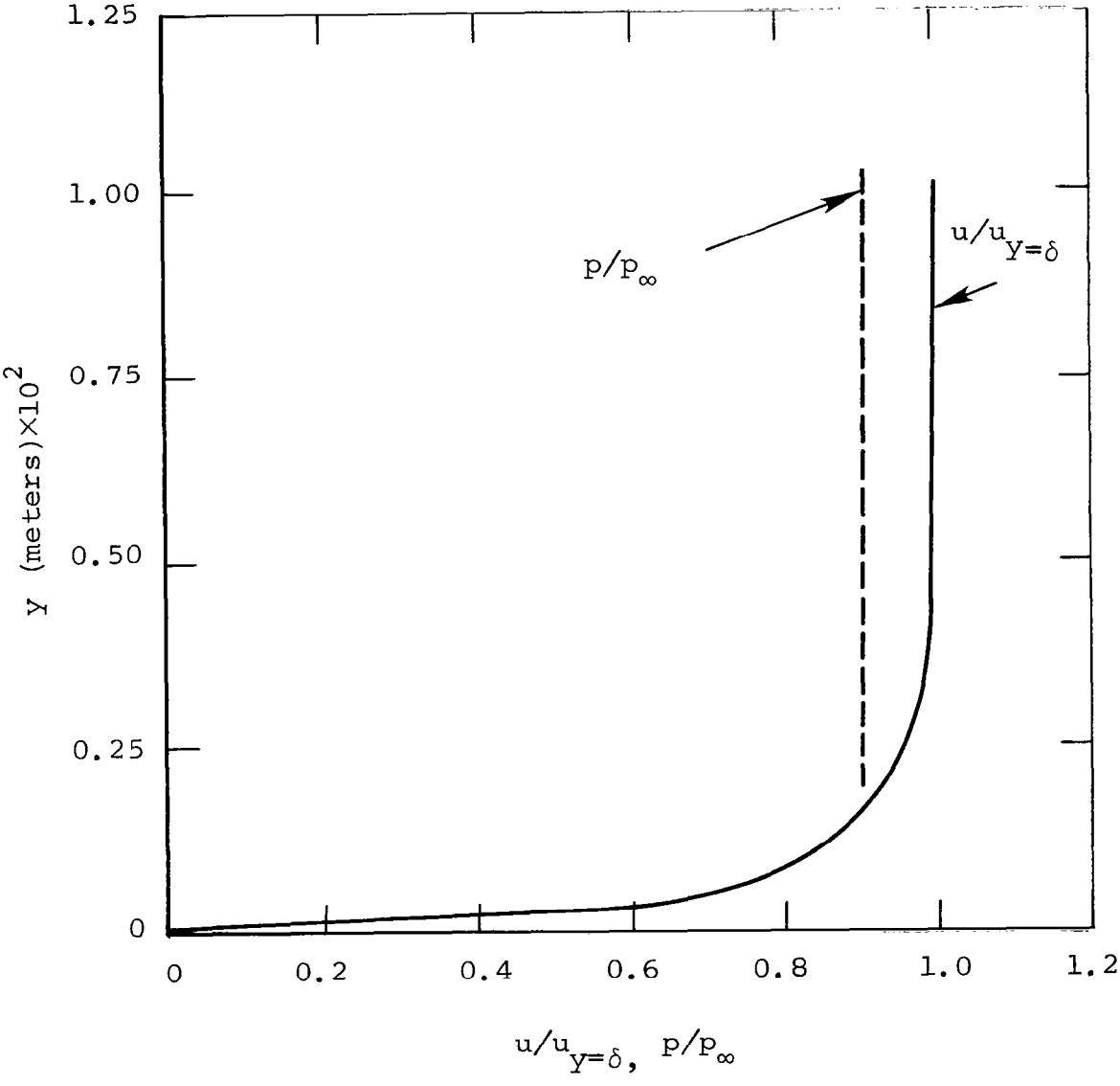

Figure 24.- Velocity and pressure distributions in the ramp boundary layer at x = 1.88 meters.

1. Report No.	2. Government Accession No.	3. Recipient's Catalog No.
NASA CR-3413		

4. Title and Subtitle	5. Report Date
An Implicit Method for the Calculation of Inlet Flow Fields	June 1981
	6. Performing Organization Code: 611/C
7. Author(s): Sedat Biringen and O. J. McMillan	8. Performing Organization Report No.: NEAR TR 232
	10. Work Unit No.
9. Performing Organization Name and Address: Nielsen Engineering & Research, Inc., 510 Clyde Avenue, Mountain View, California 94043	11. Contract or Grant No.: NAS1-15951
12. Sponsoring Agency Name and Address: National Aeronautics and Space Administration, Washington, D. C. 20546	13. Type of Report and Period Covered: Contractor Report, 9/12/79 - 11/30/80
	14. Sponsoring Agency Code

15. Supplementary Notes
Langley Technical Monitor: Wallace C. Sawyer
Topical Report

16. Abstract

Inlet flow fields are calculated by an implicit, time-marching procedure to solve the thin-layer Navier-Stokes equations formulated in body-fitted coordinates. Because the method can be used for a flow field with both subsonic and supersonic regions, it is applicable to subcritical as well as supercritical inlet operation.

Results are presented and discussed for an inlet of current design practice. Results include inviscid calculations performed for supercritical inlet operation with uniform and nonuniform inflow boundary conditions as well as for subcritical inlet operation with uniform inflow boundary conditions. Results for viscous calculations performed for supercritical inlet operation with uniform inflow boundary conditions are also discussed.

17. Key Words (Suggested by Author(s))	18. Distribution Statement
Calculation method Inlets Inviscid flow Supersonic flow Viscous flow	Unclassified - Unlimited Subject Category 02

19. Security Classif. (of this report)	20. Security Classif. (of this page)	21. No. of Pages	22. Price
Unclassifed	Unclassified	46	A03

For sale by the National Technical Information Service, Springfield, Virginia 22161

NASA-Langley, 1981